

# PaintNet: 3D Learning of Pose Paths Generators for Robotic Spray Painting

Gabriele Tiboni<sup>1</sup>, Raffaello Camoriano<sup>1</sup> and Tatiana Tommasi<sup>1</sup>

**Abstract**—Optimization and planning methods for tasks involving 3D objects often rely on prior knowledge and ad-hoc heuristics. In this work, we target learning-based long-horizon path generation by leveraging recent advances in 3D deep learning. We present PaintNet, the first dataset for learning robotic spray painting of free-form 3D objects. PaintNet includes more than 800 object meshes and the associated painting strokes collected in a real industrial setting. We then introduce a novel 3D deep learning method to tackle this task and operate on unstructured input spaces—point clouds—and mix-structured output spaces—unordered sets of painting strokes. Our extensive experimental analysis demonstrates the capabilities of our method to predict smooth output strokes that cover up to 95% of previously unseen object surfaces, with respect to ground-truth paint coverage. The PaintNet dataset and an implementation of our proposed approach will be released at <https://gabrieletiboni.github.io/paintnet/>.

## I. INTRODUCTION

Interacting with free-form 3D objects while solving complex tasks is a central problem in robotics. Grasping and manipulation are only a few examples of these tasks, together with many others that have a significant impact on industrial applications. Among them, the tasks which unfold over long time horizons are particularly challenging and require large amounts of computational resources for optimization and planning. Possible solution strategies consist in designing new tailored learning models that can effectively represent the 3D objects while managing high-dimensional structured predictions under the guidance of expert supervision.

In this work, we put under the spotlight the long-horizon task of robotic spray painting of 3D objects. Since its introduction in production lines four decades ago [1], robotic spray painting has been progressing from the development of large and expensive robotic cells for painting high volumes of identical products, to smaller and more affordable systems suitable for processing small batches of diverse objects. This has been underpinned by the development of more flexible trajectory generation paradigms, since manual programming of painting trajectories can be too expensive and time consuming to be profitable on small production batches. Such limitation has been tackled with two main approaches: programming by demonstration (PbD), and trajectory optimization and planning. In PbD, the robotic manipulator can be either directly moved along the desired task

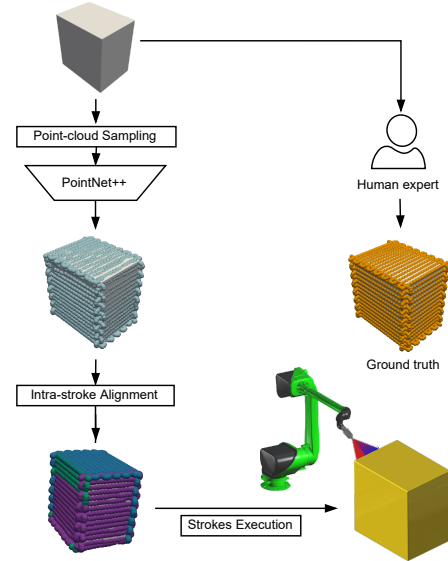


Fig. 1: Multi-stroke prediction of 6D-pose spray painting path given a raw 3D cuboid in input. The results are compared to the ground truth, hand-crafted trajectory for the same object. Different colors highlight separate—yet intersecting—painting strokes.

trajectory (kinesthetic teaching), or teleoperated by a human expert [2]. On the other hand, trajectory optimization and planning methods employ in-depth domain knowledge both to define performance measures and to update trajectory candidates [3], [4]. However, both these approaches suffer from low generalization and adaptability: they do not easily manage new diversified objects with complex shapes.

Thus, despite its practical relevance for product manufacturing, the spray painting task currently lacks a reliable and affordable solution and it is still a largely understudied problem. Part of the reason lies in the limited scope (*e.g.*, mainly planar or convex surfaces) and the proprietary nature of the data used in the existing research studies, which prevent extensive benchmarks.

With the purpose of offering a new impulse to research on this topic, we present three main contributions:

- We introduce PaintNet, the first supervised dataset for learning robotic spray painting paths generators for complex 3D objects. PaintNet includes a total of 845 object meshes covering a wide range of object shapes with growing complexity. Each object is paired with a set of painting pose paths collected in a real-world industrial scenario.

\*This work was supported by the EFORT group, providing the authors with domain knowledge, original object meshes, trajectory data, and access to the proprietary spray painting simulator used during the experiments. We also acknowledge the support of the European H2020 Elise project ([www.elise-ai.eu](http://www.elise-ai.eu)).

<sup>1</sup>Politecnico di Torino, Turin, Italy [first.last@polito.it](mailto:first.last@polito.it)

- We propose to frame the task as a 3D learning problem (see Fig. 1). We leverage the growing deep learning literature in this area that has shown excellent results for object classification, semantic segmentation, shape completion, and is proficiently used in several robotics open problems such as grasp pose prediction [5], [6]. Specifically, we develop a 3D learning pipeline that takes an object’s 3D point cloud as input and provides as output a set of sequences composed by 6D poses. Every pose describes the position and orientation of the spraying gun, while every sequence is a stroke composing the set of spraying paths.
- We define a reproducible experimental framework with quantitative and qualitative metrics that allows extensive comparisons. Our preliminary analysis includes thorough ablation studies and shows promising results.

We expect this work to pave the way to 3D learning for long-horizon path generation with potential impact even on other robotics applications beyond spray painting. Indeed, the task presents relevant open challenges, such as learning from non-unique example trajectories and simultaneously predicting unordered sets of stroke paths of varying cardinality.

## II. RELATED WORK

### A. Trajectory Planning for Robotic Spray Painting

Several existing research works on spray painting focus on matching the sprayed workpieces with a combination of geometric components which are collected in a library of references [3], or in the form of geometric primitives [7] and simple basic surfaces [8], [9], [10]. The components are associated with painting strokes which are then merged after the geometric matching to the object. More recently a point cloud slicing technique has been adopted in [11] to model the object surface. Raster paths along different axes are sampled to define the spray painting trajectories.

If the CAD model and process parameters are available, classical parametric approaches can be employed to generate trajectories [12]. Given an initial trajectory candidate, [4] optimizes a painting quality objective function by adapting trajectory waypoints and velocities.

In [13], stroke trajectories are incrementally generated and optimized by a genetic algorithm based on the outcome of previous strokes. Reinforcement learning (RL) has also been recently proposed for training painting trajectory generators by optimizing a target painting-quality reward. For example, RL for stroke sequencing proved successful for reconstructing complex planar raster images [14], while preliminary results for a simplified spray-painting task are reported in [15]. Also Self-supervised learning showed to be effective for data-driven planning in non-uniform painting of 3D surfaces with aerial robots [16]. Still, this scenario does not consider all-round 3D objects, and it is significantly different from our target industrial painting scenario.

We remark that the availability of realistic spray-painting simulators plays a significant role for trajectory optimization. Commercial (private) solutions are available, and several

works present process models and quality metrics for spray-painting simulation [17], [18], [19], [20].

### B. Deep Learning on 3D Data

Deep learning has achieved remarkable performance in various computer vision tasks both on 2D and 3D data. The latter can be formalized in different ways, with consequently different architectures: early deep networks for 3D data exploited voxel representations of object volume occupancy [21] or multiple 2D views of the object [22].

Point clouds are unstructured sets of 3D points generally obtained with 3D scanners. The PointNet architecture [23] has been successfully applied to 3D object classification and semantic segmentation. Its improved version PointNet++ [24] is better able to capture local object features. The most recent point cloud-based models effectively tackle complex high-dimensional 3D tasks, including 3D shape completion [25], [26], [27], [28], [29] and robot grasp pose generation [5], [30], [31], [32], [33], [6], [34]. In this work, we extend deep 3D learning approaches to long-horizon path planning of multiple robotic spray painting strokes.

## III. THE PAINTNET DATASET

We introduce the PaintNet dataset to accelerate research on supervised learning for multiple pose paths prediction on arbitrary 3D objects. We remark that with the term *pose* we refer to the 6D combination of Cartesian position and orientation. Therefore, a *pose path* denotes a sequence of poses, also called *stroke*.

The data consists of pairs of an object shape  $O$  and its corresponding spray painting paths set  $T$ . Each object shape is a triangular mesh  $O = (V, F)$  defined by vertices  $V \in \mathbb{R}^{|V| \times 3}$  and faces  $F$ . The three coordinates of each vertex are expressed in real-world millimeter scale. The paths set is formalized as a set of sequences  $T = \{\mathbf{t}^i\}_{i=1}^I$ . Each sequence is a *stroke*, varying in length and number across objects:  $\mathbf{t}^i$  encodes the spray painting gun position and orientation along the stroke, containing a variable number of poses  $t_{n=1, \dots, N_s}^i \in \mathbb{R}^6$ . More precisely, we record positions (3D) as the ideal paint deposit point—12cm away from the gun nozzle—and gun orientations (3D) as Euler angles. Each pose is collected by sampling from the end-effector kinematics at a rate of 4ms during offline program execution.

The data was generously collected by the EFORT group<sup>1</sup> and later preprocessed by the authors. The PaintNet dataset currently covers four object categories presented in the following order of growing complexity.

**Cuboids:** this confined class of 3D objects allows to test models under minimal generalization requirements and simpler ground truth pose paths assumptions. In particular, this category contains 300 rectangular cuboid-shaped meshes varying in height and depth—uniformly sampled in [500, 1500]mm—with width fixed at 1000mm. The corresponding spray paths have been generated offline through a simple raster pattern design, with a fixed number of 6

<sup>1</sup><https://efort.com.cn/en/index.php/group>

strokes per mesh designed to paint the exterior surface of the cuboids.

**Windows:** 145 window-like 3D meshes from real-world use cases are provided, together with their hand-crafted spray painting paths. In contrast with the previous class, this set of objects introduces harder challenges for path generation, such as predicting a non-stationary number of strokes, and handling non-trivial gun orientations.

**Shelves:** we release 312 shelf-like objects to investigate path generation approaches for highly concave surfaces, a surprisingly understudied setting in robotic spray painting. Indeed, such surface types likely require global geometric information for accurately generating a path—*e.g.*, dealing with separate surface patches alone may lead to unfeasible global patterns where the gun interferes with surrounding patches. Shelf meshes are provided in different sizes and variable number of inner shelves. Their ground truth spray pose paths have been generated through task-specific, proprietary heuristics.

**Containers:** a set of 88 industrial containers is finally included to test the generalization capabilities of deep learning-based methods. This category includes meshes with fairly heterogeneous geometric properties, and poses challenges in terms of surface convexity and object generalization under limited data. Moreover, as ground-truth paths have been manually designed by experts, the corresponding trajectories may contain inconsistencies across the dataset. This limitation requires methods to deal with the redundant nature of the 6D Cartesian spray painting task.

All object meshes are already provided in a subdivided, smoothed watertight [35] version to avoid sharp edges and holes. Moreover, any private information (*e.g.*, original logos) was accurately anonymized. An overview of the characteristics of the dataset together with some of its instances is provided in Tab I. We expect the list of object categories and number of observations per category to grow over time, as more data will be released in the future when it becomes available.

## IV. METHOD

### A. Method Overview

We propose to approach the multiple pose paths spray painting problem as a point cloud-based inference task, and present a tailored deep learning model to deal with mixed-structured output spaces.

The input point cloud can be obtained by laser scanning the workpiece to be sprayed, which avoids the need for the exact CAD model from the object designer. When the object mesh is available, as in our case, the point cloud is simply generated by sampling from the known surface, *e.g.*, through Poisson Disk sampling [36]. Unlike point clouds or sequences alone, the painting paths set is a mixture of structured (strokes) and unstructured (unordered collections of strokes of varying cardinality) components. Such nature prevents us from approaching the problem as a direct stroke prediction task. To manage this issue, we design the model output as a set of mini-sequences, which are intended to be

subsets of the original strokes. The fixed length  $\lambda \in \mathbb{N}^+$  of each mini-sequence is a parameter of the model. An optimal trade-off between the number of predicted mini-sequences and the mini-sequence length can inherently cope with the varying number of unordered strokes and varying stroke lengths. By the same logic, the ground-truth paths set is also decomposed in mini-sequences and used as a reference for the training process. The final objective of the deep learning model consists in predicting a set of mini-sequences that resembles the ground truth by being close to the original strokes and smoothly aligned with one another.

### B. Mini-sequence Model

We indicate with  $\mathbf{S} = \{\mathbf{s}^k\}_{k=1}^K$  the set of mini-sequences composed of  $\lambda$  ordered poses obtained from the ground truth strokes, with  $\mathbf{s}^k \in \mathbb{R}^{\lambda \times 6}$ . Specifically, we consider an overlap of one pose among consecutive within-stroke mini-sequences to encourage contiguous predictions, resulting in a total number of ground-truth mini-sequences  $K = \sum_{i=1, \dots, I} \lfloor N_i - \lambda + 1 \rfloor + 1$ .

Our approach takes as input the object point cloud  $\mathbf{X}$  composed of unordered 3D points  $x_{p=1, \dots, P} \in \mathbb{R}^3$ , and provides as output a set of mini-sequences  $\mathbf{Y} = \{\mathbf{y}^k\}_{k=1}^{K^*}$ , each of which contains  $\lambda$  ordered poses  $y_{l=1, \dots, \lambda}^k \in \mathbb{R}^6$ . Note that here  $K^* = \lfloor (\sum_{i=1, \dots, I} N_i) - \lambda + 1 \rfloor + 1$ , is chosen as an upper bound to fit all the input instances.

The learning objective is pursued by minimizing the following loss:

$$\mathcal{L}_{y2s} = \frac{1}{K^*} \sum_{\mathbf{y} \in \mathbf{Y}} \min_{\mathbf{s} \in \mathbf{S}} \|\mathbf{y} - \mathbf{s}\|_2^2 + \frac{1}{K} \sum_{\mathbf{s} \in \mathbf{S}} \min_{\mathbf{y} \in \mathbf{Y}} \|\mathbf{s} - \mathbf{y}\|_2^2. \quad (1)$$

In words, this symmetric version of the Chamfer Distance [37] drives mini-sequences close to the ones in the ground truth, while maximizing the ground truth mini-sequence coverage. A weight vector is introduced during norm computation to properly combine the location and orientation distance.

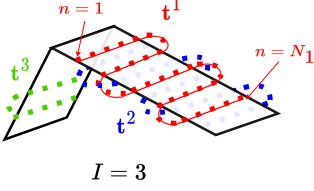
Considering that ground truth mini-sequences are overlapping, thus connected to each other within each stroke, we would like to encourage a similar behavior in the model predictions<sup>2</sup>. To this end, we introduce two sets of poses:  $\mathcal{B} = \{y_1^k\}_{k=1}^{K^*}$  and  $\mathcal{E} = \{y_\lambda^k\}_{k=1}^{K^*}$ . They respectively collect the beginning and ending poses of every predicted mini-sequence and we guide their prediction so that they attract each other via the following Chamfer-based loss:

$$\mathcal{L}_{b2e} = \frac{1}{2K^*} \left\{ \sum_{y_1^k \in \mathcal{B}} \min_{y_\lambda^j \in \mathcal{E}} \|y_1^k - y_\lambda^j\|_2^2 + \sum_{y_\lambda^k \in \mathcal{E}} \min_{y_1^j \in \mathcal{B}} \|y_\lambda^k - y_1^j\|_2^2 \right\}, \quad (2)$$

with  $j \neq k$ . Overall, we train the model to optimize  $\mathcal{L} = \mathcal{L}_{y2s} + \alpha \mathcal{L}_{b2e}$ , with  $\alpha \in \mathbb{R}^+$  being a problem-specific trade-off parameter.

<sup>2</sup>This also facilitates the intra-stroke alignment of generated mini-sequences at the post-processing stage, as discussed in Section IV-C.

TABLE I: A summary overview of the PaintNet dataset. The schematic illustration on the left shows a simple 3D object with three painting strokes, each composed of an ordered sequence of 6D poses. On the right, we show representative examples of each object class with their corresponding painting paths. The bottom part of the table presents some statistics of the dataset, by reporting five-number summaries: (min, 1<sub>st</sub> quartile, **median**, 3<sub>rd</sub> quartile, max).



|                                | Cuboids                            | Windows                           | Shelves                            | Containers                         |
|--------------------------------|------------------------------------|-----------------------------------|------------------------------------|------------------------------------|
| num. of meshes                 | 300                                | 145                               | 312                                | 88                                 |
| num. of strokes $I$            | 6                                  | (5, 7, <b>7</b> , 10, 31)         | (11, 11, <b>17</b> , 23, 131)      | (8, 13, <b>15</b> , 17, 33)        |
| stroke length $N_i$ ( $10^3$ ) | (2.6, 5.9, <b>7.5</b> , 9.4, 14.9) | (0.1, 0.5, <b>0.9</b> , 2.0, 6.0) | (0.6, 1.9, <b>3.0</b> , 5.1, 16.5) | (0.2, 1.0, <b>1.6</b> , 2.9, 12.3) |

### C. Intra-stroke Alignment

Although offline spray painting simulation allows for the execution of disconnected mini-sequences separately, this may lead to problematic cycle times on real hardware. To this end, we propose to link predicted mini-sequences for generating smooth paths while keeping different strokes correctly separated. The links will correspond to oriented edges and the final stroke can be interpreted as a weakly connected graph composed of mini-sequences as nodes. This is obtained by evaluating the distance  $d_k = \min_j \|y_\lambda^k - y_1^j\|_2^2$  with  $j \neq k$ , and connecting the two mini-sequences with a directed edge from  $k$  to  $j$  in case  $d_k$  falls below a defined threshold  $\tau$ . Finally, we merge—via averaging—the ending and beginning poses of the two mini-sequences at hand, leveraging the redundant overlapping poses induced in the training process for smoothing purposes.

In line with offline robot programming, we manually select the threshold parameter  $\tau$  to achieve optimal qualitative stroke reconstruction while preserving spray painting coverage (see Section VI-D). Note that the  $\tau$  selection procedure can potentially be automated (e.g., by cross validation) and customized to take into account additional constraints, such as desired spray painting thickness quality and enforcement of acyclic connected components.

## V. EVALUATION METRICS

To assess the performance of our approach we consider two main metrics.

**Pose-wise Chamfer Distance (PCD).** It evaluates the similarity between the prediction and the ground truth by comparing them as two clouds of poses. This metric accounts for the predicted gun positions and orientations, while disregarding the structured nature of the predictions, *i.e.*, the connectivity among poses. This allows us to fairly compare the predicted poses of models trained with different  $\lambda$ .

**Paint Coverage (PC).** Although not directly optimized at training time, we wish to assess the percentage of surface covered by the predicted strokes when executed on a spray painting simulator, relative to the ground truth. We start by defining a per-mesh painting thickness threshold above which a vertex is identified as covered—chosen as the 10<sub>th</sub> percentile of non-zero ground-truth thickness values for the mesh in question. Then, on the subset of covered ground-truth vertices, we evaluate the percentage of vertices covered when executing our predicted strokes. Note how this metric is independent of the specific spray gun model parameters used during simulation—*e.g.*, paint flux—thus suitable for benchmarking purposes.

## VI. EXPERIMENTS

### A. Implementation Details

Our pipeline leverages an encoder architecture based on PointNet++ [24], that acts as a feature extractor from the input point cloud of 5120 down-sampled 3D points to a latent space of dimensionality 1024. A 3-layer MLP is then appended to generate output poses, with hidden size (1024, 1024) and output size  $(\lambda \times 6) \times K^*$ . We apply an L2-normalization to the output orientation vectors, effectively encoding orientations as point normals. This compact representation is permitted by our conic spray gun model in simulation, which is invariant to rotations around the approach axis. To cope with limited training data, we initialize our network with pre-trained weights from a shape classification task on ModelNet [38]. As PaintNet comes with four different categories of varying complexity and structure, we carry out separate trainings for each class, while keeping the same hyperparameters. This also allows us to measure the robustness of our pipeline on multiple object categories. Input point clouds and ground truth paths are normalized during training by independently centering to zero mean and down-scaling by a category-specific factor.

TABLE II: **Left:** Predicted mini-sequences visualization for varying length  $\lambda$  on PaintNet test instances (light blue) and the corresponding ground-truth strokes (orange). **Right:** Spray painting coverage visualization based on the predicted mini-sequences for varying length  $\lambda$  and corresponding ground-truth coverage.

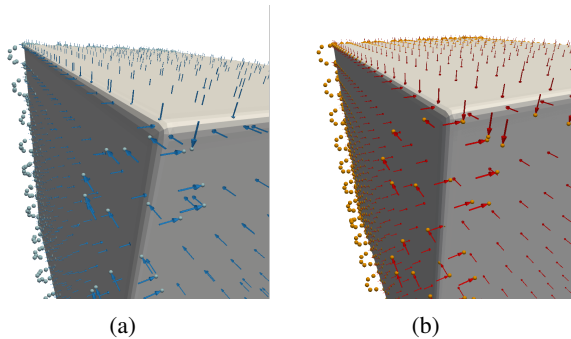
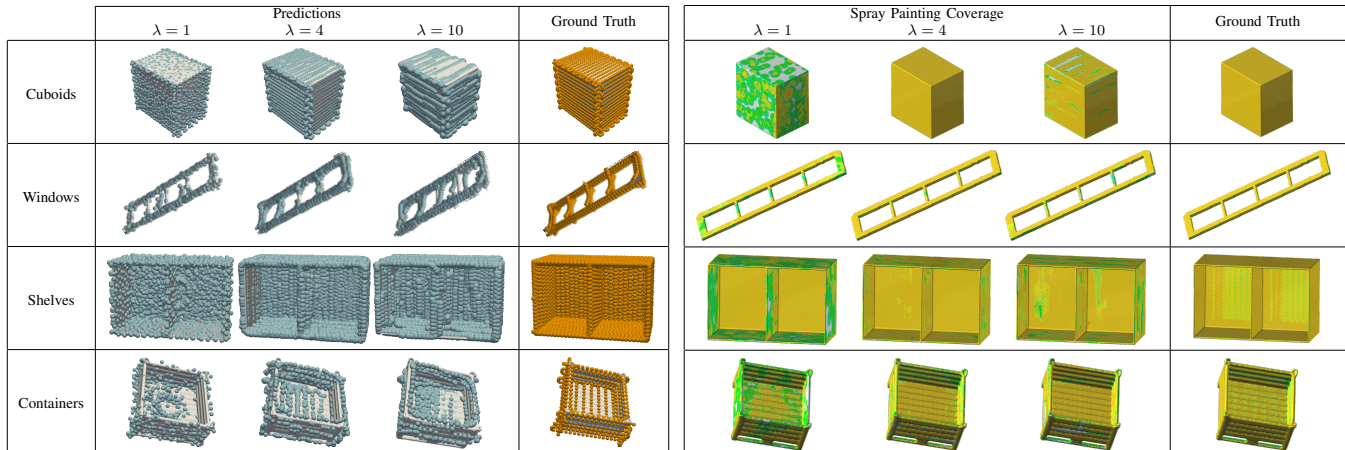


Fig. 2: (a) predicted 6D-poses vs. (b) ground-truth 6D-poses ( $\lambda = 4$ ). The original task-specific point normals are efficiently preserved and learned.

Overall, we optimize our proposed loss function  $\mathcal{L}$  with  $\alpha = 0.5$ , normals weighted by 0.25, learning rate  $10^{-3}$ , Adam optimizer, and 1250 epochs. Rather than directly dealing with poses densely sampled every 4ms, we reduce the output dimensionality by down-sampling ground truth trajectories at a lower frequency. The number of obtained total poses per object category is indicated in the header of Table III. Finally, we randomly split all four categories into a training and a test set, with respective proportions of 80%-20%. All results reported in the manuscript are computed on previously unseen test instances. Additional results and visualizations are reported in the accompanying video.

### B. Results: Mini-sequence Inference

We carry out a thorough analysis on the quality of the mini-sequences predicted by our trained model under varying  $\lambda$  values. By doing so, we may investigate how a direct set-to-set task ( $\lambda = 1$ ) would perform, in comparison with our mini-sequence model ( $\lambda > 1$ ). For clear reasons, the  $\mathcal{L}_{b2e}$  loss term and overlapping component are not taken into account with  $\lambda = 1$ , which effectively reduces to a Chamfer-based multi-pose generation task. We report qualitative re-

|                | Cuboids<br>(2000) | Windows<br>(500) | Shelves<br>(4000) | Containers<br>(1000) |
|----------------|-------------------|------------------|-------------------|----------------------|
| $\lambda = 1$  | 959,29            | 950,72           | 455,74            | 1,073,15             |
| $\lambda = 4$  | <b>18,25</b>      | <b>57,17</b>     | <b>36,65</b>      | <b>274,84</b>        |
| $\lambda = 10$ | 37,98             | 118,50           | 56,06             | 364,54               |

TABLE III: Pose-wise Chamfer Distance averaged over each category’s test set, scaled by  $10^4$ . The number of effective down-sampled ground-truth points is reported in parenthesis.

|                | Cuboids<br>(2000) | Windows<br>(500) | Shelves<br>(4000) | Containers<br>(1000) |
|----------------|-------------------|------------------|-------------------|----------------------|
| $\lambda = 1$  | 5.42%             | 39.90%           | 26.40%            | 71.99%               |
| $\lambda = 4$  | <b>95.30%</b>     | <b>84.05%</b>    | <b>73.03%</b>     | <b>89.32%</b>        |
| $\lambda = 10$ | 79.64%            | 68.84%           | 70.88%            | 82.88%               |

TABLE IV: Spray painting coverage quantitative results: percentage of covered mesh vertices with respect to ground-truth trajectories. Results are averaged over the test set.

sults on a subset of test instances in Tab. II (Left), and the full quantitative results on the test set in terms of PCD in Tab. III. Our analysis shows that a direct set-to-set task leads to highly sparse, unordered data, which does not resemble the original strokes. On the other hand, our method show promising results by simply predicting mini-sequences rather than individual poses, effectively learning and preserving the desired output structure. Note that overly large values of  $\lambda$  may hinder the results, as in the case of  $\lambda = 10$  in our experiments. We suspect this phenomenon to be caused by learning on fixed permutations of long ground truth mini-sequences, which can make it hard for the network to find a general pattern. Nevertheless, we observe that a best trade-off can be obtained with  $\lambda = 4$ , which turns out to be optimal on all object categories by means of PCD. Finally, we report a close-up illustration of predicted poses vs. ground-truth poses in Fig. 2, demonstrating successful learning of positions and normals at the same time, even when strokes locally intersect each other.

### C. Results: Spray Painting Coverage

As intra-stroke alignment may result in over-optimistic coverage percentages due to wrongly connected sequences, we first perform a thorough paint coverage analysis on the sole, disconnected network predictions. Note how, even though predictions lack inter-sequence connections at this stage, the overlapping component allows—at least in theory—a smooth spray gun transition from one sequence to another, without skipping steps. We therefore obtain a painting feedback by simply executing each predicted mini-sequence in simulation in a random permutation. On the other hand, ground truth paint thickness references are obtained through the execution of the known long-horizon trajectory. A proprietary simulator developed by the EFORT group is used for this step, but similar tools may equally serve the scope [13]. Qualitative results on a few instances of PaintNet are depicted in Table II (Right), with a color map design that matches our paint coverage metric defined in Sec. V—*i.e.*, vertex thicknesses higher than a relative threshold visually appear the same. Quantitative paint coverage values are reported in Table IV, averaged over all instances of each category’s test set. In general, we draw similar conclusions to the case of mini-sequence inference: direct set-to-set learning falls short ( $\lambda = 1$ ), while an optimal value  $\lambda = 4$  allows for up to 95.30% relative surface coverage and best overall coverage across all four object categories. These results importantly demonstrate that supervised learning is a promising approach for learning the downstream task from expert data, rather than directly optimizing for spray painting coverage.

### D. Results: Intra-stroke Alignment

We finally inspect the outcome of our post-processing step in the attempt to reconstruct longer strokes for practical execution on robotic systems. By design, our training pipeline already encourages the prediction of overlapping mini-sequences and allows a simple technique based on graph connected components to be applied, avoiding complex ordering procedures. We demonstrate the effectiveness of the intra-stroke alignment step in Fig. 3, highlighting the contribution of both the mini-sequence attraction loss  $\mathcal{L}_{b_{2e}}$  and overlapping component to obtain optimal qualitative and quantitative results. In particular, we note that paint coverage results are preserved after the intra-stroke alignment step, albeit not exactly the same—likely due to the merging of overlapping poses and smoothing.

## VII. DISCUSSION

Our experimental evaluation shows that aggregating poses into overlapping mini-sequences is a winning strategy: with respect to the naïve set-to-set approach ( $\lambda = 1$ ), it allows to preserve the desired output structure and successfully deal with the high-dimensional and mix-structured nature of ground-truth paths. Our method yields consistent accuracy and paint coverage performances with the same mini-sequence length  $\lambda$  across different PaintNet object categories. Furthermore, the internal sequencing of output strokes can

| ✗ attraction, overlapping   | ✓ attraction, overlapping  | ✗ attraction, overlapping   | ✓ attraction, overlapping   | ground truth  |
|---|--|---|---|---|
| ✗ intra-stroke al.  | ✓ intra-stroke al.   | ✗ intra-stroke al.  | ✓ intra-stroke al.  |   |
|  |  |  |  |  |
| PC = 75.06%   | PC = 72.29%  | PC = 98.32%   | PC = 97.94%   | PC = 100%   |
|  |  |  |  |  |
| PC = 87.70%   | PC = 87.51%  | PC = 93.13%   | PC = 92.83%   | PC = 100%   |

Fig. 3: Results of the intra-stroke alignment post-processing step ( $\tau = 0.15$ ) on cuboids and windows, obtained with best value  $\lambda = 4$ . This ablation study shows the effectiveness of the attraction loss term and overlapping component to reconstruct long-horizon strokes.

be reconstructed via a simple post-processing procedure, resulting in longer strokes that can be practically tracked by painting robots. We finally demonstrate the applicability and effectiveness of our method in simulation, achieving up to 95% average paint coverage with no significant deterioration caused by post-processing.

## VIII. CONCLUSIONS

In this paper, we tackled the core robotic problem of long-horizon, multiple path generation for tasks involving free-form 3D objects. To this aim, we focused on robotic spray painting as a particularly well-suited task in such domain. In this context, we introduce PaintNet, the first industry-grade supervised dataset for robotic spray painting, including four object categories of increasing complexity and shape variety. PaintNet is aimed at fostering research in this challenging setting by providing real-world benchmark data which would otherwise be hard to acquire for robot learning researchers. Moreover, we present the first method for learning the underlying task by building on recently developed 3D deep learning architectures. We validate the method on the PaintNet dataset and evaluate its performance in simulation.

Future work enabled by PaintNet will include the evaluation of more painting quality metrics beyond coverage, such as thickness accuracy deviation. Investigating learning methods incorporating painting quality feedback, including reinforcement and imitation learning, could also lead to improved performance. Evaluation of sim-to-real methods in this setting involving complex and hard-to-model paint deposition is also an interesting direction with potential impact on real-world robotic manufacturing.

## REFERENCES

- [1] H. Kiba, Y. Itoh, and K. Kiryu, “Vehicle body painting robot,” Feb. 12 1985, US Patent 4,498,414.
- [2] S. Calinon, *Robot programming by demonstration*. EPFL Press, 2009.
- [3] G. Biegelbauer, A. Pichler, M. Vincze, C. Nielsen, H. Andersen, and K. Haeusler, “The inverse approach of flexpaint [robotic spray painting],” *IEEE Robotics & Automation Magazine*, vol. 12, no. 3, pp. 24–34, 2005.

- [4] D. Gleeson, S. Jakobsson, R. Salman, F. Ekstedt, N. Sandgren, F. Edelvik, J. S. Carlson, and B. Lennartson, "Generating optimized trajectories for robotic spray painting," *IEEE Transactions on Automation Science and Engineering*, 2022.
- [5] J. Varley, C. DeChant, A. Richardson, J. Ruales, and P. Allen, "Shape completion enabled robotic grasping," in *2017 IEEE/RSJ international conference on intelligent robots and systems (IROS)*. IEEE, 2017, pp. 2442–2447.
- [6] P. Ni, W. Zhang, X. Zhu, and Q. Cao, "Pointnet++ grasping: Learning an end-to-end spatial grasp generation algorithm from sparse point clouds," in *2020 IEEE International Conference on Robotics and Automation (ICRA)*. IEEE, 2020, pp. 3619–3625.
- [7] A. Gasparetto, R. Vidoni, D. Pillan, and E. Saccavini, "Automatic path and trajectory planning for robotic spray painting," in *ROBOTIK 2012; 7th German Conference on Robotics*. VDE, 2012, pp. 1–6.
- [8] W. Sheng, N. Xi, M. Song, Y. Chen, and P. MacNeille, "Automated cad-guided robot path planning for spray painting of compound surfaces," in *IEEE/RSJ International Conference on Intelligent Robots and Systems (IROS)*, vol. 3, 2000.
- [9] H. Chen and N. Xi, "Automated tool trajectory planning of industrial robots for painting composite surfaces," *The International Journal of Advanced Manufacturing Technology*, vol. 35, pp. 680–696, 01 2008.
- [10] X. Li, O. A. Landsnes, H. Chen, M.-V. Sudarshan, T. A. Fuhlbrigge, and M.-A. Rege, "Automatic trajectory generation for robotic painting application," in *International Symposium on Robotics (ISR) and German Conference on Robotics (ROBOTIK)*, 2010.
- [11] W. Chen, X. Li, H. Ge, L. Wang, and Y. Zhang, "Trajectory planning for spray painting robot based on point cloud slicing technique," *Electronics*, vol. 9, no. 6, 2020.
- [12] S.-H. Suh, I.-K. Woo, and S.-K. Noh, "Development of an automatic trajectory planning system (atps) for spray painting robots," in *Proceedings. 1991 IEEE International Conference on Robotics and Automation*. IEEE, 1991, pp. 1948–1955.
- [13] M. Andulkar and S. Chiddarwar, "Incremental approach for trajectory generation of spray painting robot," *Industrial Robot: An International Journal*, vol. 42, pp. 228–241, 05 2015.
- [14] Z. Huang, W. Heng, and S. Zhou, "Learning to paint with model-based deep reinforcement learning," in *Proceedings of the IEEE/CVF International Conference on Computer Vision*, 2019, pp. 8709–8718.
- [15] J. Kiemel, P. Yang, P. Meißner, and T. Kröger, "Paintrl: Coverage path planning for industrial spray painting with reinforcement learning," in *RSS Workshop on Closing the Reality Gap in Sim2real Transfer for Robotic Manipulation*, 2019.
- [16] A. S. Vempati, R. Siegwart, and J. Nieto, "A data-driven planning framework for robotic texture painting on 3d surfaces," in *IEEE International Conference on Robotics and Automation (ICRA)*, 2020.
- [17] M. S. Arikan and T. Balkan, "Process simulation and paint thickness measurement for robotic spray painting," *CIRP Annals*, vol. 50, no. 1, pp. 291–294, 2001.
- [18] D. C. Conner, A. Greenfield, P. N. Atkar, A. A. Rizzi, and H. Choset, "Paint deposition modeling for trajectory planning on automotive surfaces," *IEEE Transactions on Automation Science and Engineering*, vol. 2, no. 4, pp. 381–392, 2005.
- [19] Y. Chen, W. Chen, B. Li, G. Zhang, and W. Zhang, "Paint thickness simulation for painting robot trajectory planning: a review," *Industrial Robot: An International Journal*, 2017.
- [20] J. Casanova, J. Lima, and P. Costa, "A simulation tool for optimizing a 3d spray painting system," in *Optimization, Learning Algorithms and Applications*, A. I. Pereira, F. P. Fernandes, J. P. Coelho, J. P. Teixeira, M. F. Pacheco, P. Alves, and R. P. Lopes, Eds., 2021.
- [21] C. R. Qi, H. Su, M. Nießner, A. Dai, M. Yan, and L. J. Guibas, "Volumetric and multi-view cnns for object classification on 3d data," in *Proceedings of the IEEE conference on computer vision and pattern recognition*, 2016, pp. 5648–5656.
- [22] H. Su, S. Maji, E. Kalogerakis, and E. Learned-Miller, "Multi-view convolutional neural networks for 3d shape recognition," in *Proceedings of the IEEE international conference on computer vision*, 2015, pp. 945–953.
- [23] C. R. Qi, H. Su, K. Mo, and L. J. Guibas, "Pointnet: Deep learning on point sets for 3d classification and segmentation," in *Proceedings of the IEEE conference on computer vision and pattern recognition*, 2017, pp. 652–660.
- [24] C. R. Qi, L. Yi, H. Su, and L. J. Guibas, "Pointnet++: Deep hierarchical feature learning on point sets in a metric space," *Advances in neural information processing systems*, vol. 30, 2017.
- [25] W. Yuan, T. Khot, D. Held, C. Mertz, and M. Hebert, "Pcn: Point completion network," in *2018 International Conference on 3D Vision (3DV)*. IEEE, 2018, pp. 728–737.
- [26] X. Wang, M. H. Ang Jr, and G. H. Lee, "Cascaded refinement network for point cloud completion," in *Proceedings of the IEEE/CVF Conference on Computer Vision and Pattern Recognition*, 2020, pp. 790–799.
- [27] X. Wen, T. Li, Z. Han, and Y.-S. Liu, "Point cloud completion by skip-attention network with hierarchical folding," in *Proceedings of the IEEE/CVF Conference on Computer Vision and Pattern Recognition*, 2020, pp. 1939–1948.
- [28] R. Wu, X. Chen, Y. Zhuang, and B. Chen, "Multimodal shape completion via conditional generative adversarial networks," in *European Conference on Computer Vision*. Springer, 2020, pp. 281–296.
- [29] A. Alliegro, D. Valsesia, G. Fracastoro, E. Magli, and T. Tommasi, "Denoise and contrast for category agnostic shape completion," in *Proceedings of the IEEE/CVF Conference on Computer Vision and Pattern Recognition*, 2021, pp. 4629–4638.
- [30] A. Mousavian, C. Eppner, and D. Fox, "6-dof graspnet: Variational grasp generation for object manipulation," in *Proceedings of the IEEE/CVF International Conference on Computer Vision*, 2019, pp. 2901–2910.
- [31] A. Murali, A. Mousavian, C. Eppner, C. Paxton, and D. Fox, "6-dof grasping for target-driven object manipulation in clutter," in *2020 IEEE International Conference on Robotics and Automation (ICRA)*. IEEE, 2020, pp. 6232–6238.
- [32] C. Wu, J. Chen, Q. Cao, J. Zhang, Y. Tai, L. Sun, and K. Jia, "Grasp proposal networks: an end-to-end solution for visual learning of robotic grasps," *Advances in Neural Information Processing Systems*, vol. 33, pp. 13 174–13 184, 2020.
- [33] Y. Qin, R. Chen, H. Zhu, M. Song, J. Xu, and H. Su, "S4g: Amodal single-view single-shot se (3) grasp detection in cluttered scenes," in *Conference on robot learning*. PMLR, 2020, pp. 53–65.
- [34] A. Alliegro, M. Rudorfer, F. Frattin, A. Leonardis, and T. Tommasi, "End-to-end learning to grasp via sampling from object point clouds," *IEEE Robotics and Automation Letters*, vol. 7, no. 4, pp. 9865–9872, 2022.
- [35] J. Huang, H. Su, and L. Guibas, "Robust watertight manifold surface generation method for shapenet models," *arXiv preprint arXiv:1802.01698*, 2018.
- [36] R. L. Cook, "Stochastic sampling in computer graphics," *ACM Transactions on Graphics (TOG)*, vol. 5, no. 1, pp. 51–72, 1986.
- [37] H. Fan, H. Su, and L. J. Guibas, "A point set generation network for 3d object reconstruction from a single image," in *Proceedings of the IEEE conference on computer vision and pattern recognition*, 2017, pp. 605–613.
- [38] Z. Wu, S. Song, A. Khosla, F. Yu, L. Zhang, X. Tang, and J. Xiao, "3d shapenets: A deep representation for volumetric shapes," 2014. [Online]. Available: <https://arxiv.org/abs/1406.5670>